Nanotechnology **20** (2009) 465707 (6pp) doi:10.1088/0957-4484/20/46/465707

Cosserat curve model for superelasticity of helices

L Dai and W Z Shen[1]

Laboratory of Condensed Matter Spectroscopy and Opto-Electronic Physics, Department of Physics, Shanghai Jiao Tong University, 1954 Hua Shan Road, Shanghai 200030, People's Republic of China

E-mail: wzshen@sjtu.edu.cn

Received 22 April 2009, in final form 13 September 2009
Published 22 October 2009
Online at stacks.iop.org/Nano/20/465707

Abstract

Superelasticity behavior of helices has been the focus of recent research in micro-/nano-engineering, while the traditional Kirchhoff rod model restricts itself in the bending and torsion conditions. With the aid of the concept of a Cosserat curve, a novel theoretical basis has been established for statics and dynamics of helices with essential extension and shear, which is able to quantitatively analyze the superelastic mechanical properties. Except for a good agreement with the experimental observation, numerical solutions have shown that we cannot only predict two important properties of the superelasticity characteristics: the breaking force and the stretch of the coil wire under the axial loading, but also precisely describe and explain the Hooke's constant and torque in the entire stretching and breaking processes. The present work has provided useful information for the future experimental investigation on superelasticity as well as its application in meta-/quantum devices.

(Some figures in this article are in colour only in the electronic version)

As three-dimensional structures of helicity and periodicity, micro-/nanohelices constitute a broad and active research field in micro-/nano-engineering [1–4]. In particular, their superelasticity behavior has attracted considerable attention in recent years [5–7], which describes the phenomenon of a micro-/nanohelix elastically recovering its original shape from an extremely large axial extension to its limit. The mechanical properties of superelasticity afford quite a lot of opportunities for the assembly of meta-/quantum devices with a large number of potential applications [5–8], notably in elastic energy storage, resonating generator, reinforcement in high-strain composites, electromagnetic wave absorbers and other related areas benefiting from the good elastic recovery. A case in point is the microwave nanoantennas that have large bandwidths with an available high resonance frequency [8].

The superelasticity phenomenon was first found in a carbon nanocoil [5] through the loading and unloading experiments performed by atomic force microscopy. The maximum relative elongation of the nanocoil reached ∼42% and a Hooke's constant of 0.12 N m^{-1} in the low-strain region was recorded. Gao *et al* [6] succeeded in increasing the elongation to as large as ∼70% in the ZnO nanohelix and attributed the superelasticity to the small thickness and the superlattice structure of the nanohelix. In order to test the endurance of the superelasticity behavior, Cao *et al* [7] have performed on Si_3N_4 microcoils the effect of repeating loading on the shape recovery and further extended the load–elongation relation to the entire stretching and breaking processes. An extraordinary elongation of 80–300% was reported.

However, the current theoretical works fail in presenting a complete and accurate description of the superelasticity phenomenon. With a derived Hooke's constant, the classical elasticity theory [5, 6] only qualitatively describes the elastic properties of helices in part of the stretching process. It neither gives a direct explanation of the loading experiments nor considers the other important mechanical quantities, such as the breaking force of loading, stretching of the coil wire and torque. As a more widely used theory for continuous rods, the Kirchhoff rod model provides an approach to study the statics and dynamics of elastic thin rods of all kinds ranging from climbing plants [9, 10] and the filamentary structures of biomolecules [11–13] to the micro-/nanohelices [14, 15],

[1] Author to whom any correspondence should be addressed.

but it restricts itself to the hypothesis of an inextensible and unshearable rod, and is no use for superelasticity research under high-stress loading.

In this paper, we establish a novel theory for the superelasticity of micro-/nanohelices in the entire stretching and breaking domain by employing the concept of the extensible and shearable Cosserat curve [16]. The Cosserat curve model, reduced into the Kirchhoff rod model in the low-strain region, cannot only quantitatively explain all the experimental observation in the literature, but also offers the detailed mechanical quantities of the helical system, such as the breaking force, stretching of coil wires, Hooke's constant and torque. We have demonstrated that the Cosserat curve model provides a complete theoretical framework to study the superelasticity behavior of micro-/nanohelices.

The concept of the Cosserat curve was first introduced by Cosserat *et al* [17] for a directed curve with an orthonormal triad of directors and specified by four vector fields. Whitman and DeSilva [16] further developed the theory of the curve as a special case of the nonlinear dynamical theory of elastic directed curves and gave the basic equilibrium equations:

$$\hat{\tau}_\alpha - \varepsilon_{\alpha\beta\gamma}\tau_\beta W_\gamma = 0, \tag{1a}$$

$$\hat{m}_\alpha - \varepsilon_{\alpha\beta\gamma}(m_\beta W_\gamma + \tau_\beta y_\gamma) = 0, \tag{1b}$$

where τ and m are the total force and torque across the cross section of the curve, respectively, ε is the permutation tensor, and W and y are the director and position deformation measures, respectively. The Greek subscripts α, β and γ take on the values 1, 2 and 3. $\hat{(\,)} = \partial/\partial S = \lambda\dot{(\,)} = \lambda\partial/\partial s$ and $\lambda = \partial s/\partial S$ is the stretch of the curve with S the arc length along a fixed reference configuration and s the one along a deformed configuration.

As shown in figures 1(a) and (b), to establish the Cosserat curve model for exploring exactly the superelasticity behavior of micro-/nanohelices, we suppose that a uniform helix H_I, with the radius a_0, pitch b_0, coil wire radius r_0 and number of coils N, is loaded under a force F along its helical axis to transform to the elongated helix H_F of radius a, pitch b and coil wire radius r, where the elongation of the helix is L. In this model H_I is the fixed reference configuration and H_F is the deformed one. Figure 1(a′) presents a section of H_I and figure 1(b′) displays the corresponding elongated section of H_F with the stretching length L_S, where $\boldsymbol{D}_i$ $(i = 1, 2, 3)$, the director basis of H_I, and $\boldsymbol{d}_i$ that of H_F are defined by a set of Euler angles ϕ_0, θ_0, ψ_0 and ϕ, θ, ψ, respectively [18]. For the configuration of helix ϕ_0, θ_0, $\dot{\psi}_0$, ϕ, θ and $\dot{\psi}$ are all constants [19], and the director deformation measures $W^{(0)}$ of H_I and W of H_F have the form

$$W_1^{(0)} = -\psi_0' \sin\theta_0 \cos\phi_0, \qquad W_2^{(0)} = \psi_0' \sin\theta_0 \sin\phi_0,$$
$$W_3^{(0)} = \psi_0' \cos\theta_0, \tag{2a}$$

$$W_1 = -\hat{\psi} \sin\theta \cos\phi, \qquad W_2 = \hat{\psi} \sin\theta \sin\phi,$$
$$W_3 = \hat{\psi} \cos\theta. \tag{2b}$$

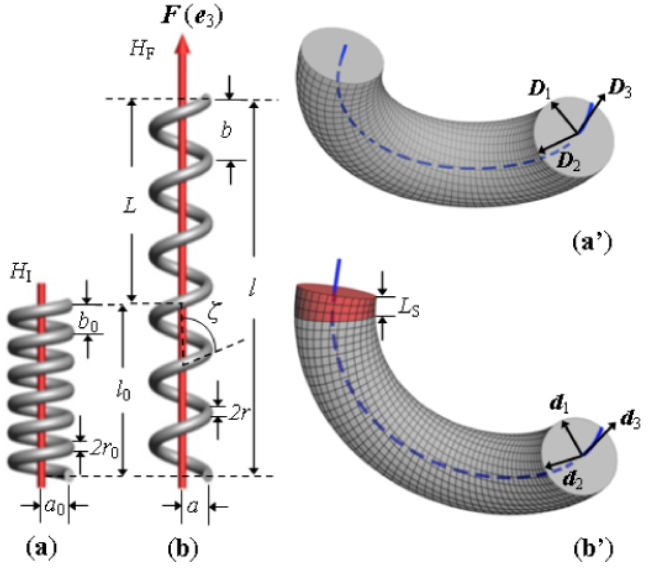

Figure 1. Configuration of a helix (a) H_I before and (b) H_F after a loading by a force F along its axis. (a′) A section of H_I and (b′) is the corresponding elongated section of H_F.

We choose the third director $\boldsymbol{D}_3$ of H_I along the tangent to the centerline of the coil wire axis. For such a case the force and torque in equation (1) yield

$$\tau_1 = E_1 y_1, \qquad \tau_2 = E_2 y_2, \qquad \tau_3 = E_3(y_3 - 1) \tag{3a}$$

$$m_1 = A(W_1 - W_1^{(0)}), \qquad m_2 = B(W_2 - W_2^{(0)}),$$
$$m_3 = C(W_3 - W_3^{(0)}) \tag{3b}$$

where $E_1 = E_2 = K_2 G\pi r_0^2$, $E_3 = E\pi r_0^2$, $A = B = EI$ and $C = GJ$. K_2 is the Timoshenko shear coefficient and is related to Poisson's ratio ν through $K_2 = [6(1+\nu)^2]/[7 + 12\nu + 4\nu^2]$ [20]. E and G are the Young's and shear moduli, respectively. $I = (\pi r_0^4)/4$ is the moment of inertia and $J = (\pi r_0^4)/2$ is the polar moment of inertia of the cross section.

The force F is assumed along the $\boldsymbol{e}_3$ axis of the fixed Cartesian basis. We use that condition in the equilibrium equation (1*b*) and obtain

$$B(\hat{W}_1 - \hat{W}_1^{(0)}) - (B - C)W_2 W_3 + B W_2^{(0)} W_3 - C W_3^{(0)} W_2$$
$$- (E_2 - E_3) y_2 y_3 - E_3 y_2 = 0, \tag{4a}$$

$$C(\hat{W}_3 - \hat{W}_3^{(0)}) + B(W_1^{(0)} W_2 - W_2^{(0)} W_1) = 0. \tag{4b}$$

Two relations of Euler angles can be determined: $\phi = \phi_0$ is obtained from equations (2) and (4*b*), while $\hat{\psi} = \dot{\psi}_0$ is derived from $\hat{\psi} = \lambda/\sqrt{a^2 + b^2}$ [16]. The position vectors obtained from equation (1*a*) of H_F satisfy

$$y_1 = -\frac{F}{E_2} \sin\theta \cos\phi_0, \qquad y_2 = \frac{F}{E_2} \sin\theta \sin\phi_0,$$
$$y_3 = \frac{F}{E_3} \cos\theta + 1. \tag{5}$$

From equation (6), we can have not only the stretching λ:

$$\lambda = \sqrt{\frac{F^2}{E_2^2} \sin^2\theta + \left(\frac{F}{E_3} \cos\theta + 1\right)^2}, \tag{6}$$

but also the radius and pitch of H_I and H_F in terms of the Euler angles:

$$a_0 = \frac{\sin\theta_0}{\dot{\psi}_0}, \qquad b_0 = \frac{2\pi\cos\theta_0}{\dot{\psi}_0}, \tag{7a}$$

$$\begin{aligned} a &= \frac{1}{\dot{\psi}_0}\left[\left(\frac{F}{E_3}\cos\theta + 1\right) - \frac{F}{E_2}\cos\theta\right]\sin\theta, \\ b &= \frac{2\pi}{\dot{\psi}_0}\left[\frac{F}{E_2}\sin^2\theta + \left(\frac{F}{E_3}\cos\theta + 1\right)\cos\theta\right]. \end{aligned} \tag{7b}$$

By virtue of equations (2) and (5) and the resultant $\phi = \phi_0$, $\hat{\psi} = \dot{\psi}_0$, equation (4*a*) can be rewritten as

$$\begin{aligned} &\left(\frac{1}{E_3} - \frac{1}{E_2}\right)\cos\theta\sin\theta F^2 + \sin\theta F - C\dot{\psi}_0^2(\cos\theta - \cos\theta_0) \\ &\quad\times \sin\theta + B\dot{\psi}_0^2(\sin\theta - \sin\theta_0)\cos\theta = 0. \end{aligned} \tag{8}$$

Following Whitman and DeSilva [16], we can further find that in our case the torque along the same direction as that of the force F obeys the expression

$$M = B\dot{\psi}_0(\sin\theta - \sin\theta_0)\sin\theta + C\dot{\psi}_0(\cos\theta - \cos\theta_0)\cos\theta. \tag{9}$$

Hooke's constant h of H_F is given by Hooke's law: $h = \mathrm{d}F/\mathrm{d}L$. From equations (7) and (8), we have the form of

$$h = -\frac{P_1 P_4}{N(P_3 P_4 + P_2)},$$

where

$$\begin{aligned} P_1 &\equiv [\dot{\psi}/2\pi]\Big/\left[1 + 2F\cos\theta\left(\frac{1}{E_3} - \frac{1}{E_2}\right)\right] \\ P_2 &\equiv 2\left(\frac{1}{E_3} - \frac{1}{E_2}\right)\cos\theta\sin\theta F + \sin\theta \\ P_3 &\equiv -\left[\frac{1}{E_2} + \left(\frac{1}{E_3} - \frac{1}{E_2}\right)\cos^2\theta\right] \\ &\quad\times\left[1 + 2F\cos\theta\left(\frac{1}{E_3} - \frac{1}{E_2}\right)\right]^{-1} \\ P_4 &\equiv \left(\frac{1}{E_3} - \frac{1}{E_2}\right)\frac{1 - 2\cos^2\theta}{\sin\theta}F^2 - \frac{\cos\theta}{\sin\theta}F + \dot{\psi}_0^2(B - C) \\ &\quad\times\frac{1 - 2\cos^2\theta}{\sin\theta} - B\dot{\psi}_0^2\sin\theta - C\dot{\psi}_0^2\cos\theta_0\frac{\cos\theta}{\sin\theta}. \end{aligned} \tag{10}$$

It turns out that with a knowledge of the geometry parameters a_0, b_0, r_0 and N of the undeformed helix H_I and the applied load force F or torque M, the radius a, pitch b, coil wire radius r and Hooke's constant h of H_F can be derived through equations (6)–(10) with the conservation of length $l = \lambda l_0$ and that of coil wire volume, where $l = N\sqrt{(2\pi a)^2 + b^2}$ and $l_0 = N\sqrt{(2\pi a_0)^2 + b_0^2}$ are the unwound length of the coil wire after and before the loading, respectively (as shown in figures 1(a) and (b)). It should be noted that we can have $E_{1,2} \to \infty$ and $E_3 \to \infty$ in the Cosserat curve model to describe the rod with infinite resistance to shear deformation and extension, respectively, where the former effect plays a more important role during the extremely large axial stretching for the superelasticity behavior of micro-/nanohelices. The Kirchhoff rod model can be easily recovered by omitting both kinds of deformation, i.e. $E_{1,2,3} \to \infty$. Through equation (8), the loading force F_K in the Kirchhoff rod model is subjected to the constraint with respect to $E_{2,3} \to \infty$:

$$F_K = \dot{\psi}_0^2\left[B\cos\theta\left(\frac{\sin\theta_0}{\sin\theta} - 1\right) + C(\cos\theta - \cos\theta_0)\right], \tag{11}$$

which leads to the Kirchhoff Hooke's constant h_K taking the particularly simple and explicit form:

$$h_K = \dot{\psi}_0^2\left[(C - B) + B\sin\theta_0\left(\frac{\cos^2\theta}{\sin^3\theta} + \frac{1}{\sin\theta}\right)\right]. \tag{12}$$

From equation (12) we can deduce the Kirchhoff Hooke's constant h_{K0} in the absence of the load:

$$h_{K0} = \frac{\dot{\psi}_0^3}{2\pi N}\left(GJ + EI\frac{\tau_0^2}{k_0^2}\right), \tag{13}$$

where $k_0 = \dot{\psi}_0\sin\theta_0$ and $\tau_0 = \dot{\psi}_0\cos\theta_0$ are the curvature and torsion, respectively. Equation (13) is consistent with the expression of Hooke's constant from the Kirchhoff rod model under the assumption $J = I$ and $G = E$ [14] (also note that λ in [6] is the same as $\dot{\psi}_0$ in the present paper). The above argument shows that the present Cosserat curve model, as the developed theory from the Kirchhoff rod model, provides a new theoretical basis for studies of the statics and dynamics of helices with the contribution of rod shear and extension.

We now demonstrate the proposed Cosserat curve model through the loading experiments of the superelasticity behavior for the two typical helices (microcoil and nanocoil). Figures 2(a) and (b) present the theoretical calculations (solid curves) of the load versus elongation, deduced from equations (7) and (8), for the Si_3N_4 microcoil [7] and carbon nanocoil [5], respectively. In the calculation, we employ the parameters of $a_0 = 80\ \mu$m, $b_0 = 200\ \mu$m, $r_0 = 2.58\ \mu$m, $N = 8$, $E = 240$ GPa [7] and $\nu = 0.25$ [21] for the Si_3N_4 microcoil, and $a_0 = 0.38\ \mu$m, $b_0 = 2\ \mu$m, $r_0 = 0.1\ \mu$m, $N = 10$, $G = 2.5$ GPa and $\nu = 0.27$ [5] for the carbon nanocoil, where the geometry parameters are all from the SEM images. To make a direct comparison, we have also shown the experimental data (squares) of the Si_3N_4 microcoil [7] and carbon nanocoil [5]. At the beginning of the loading process, as displayed in figures 2(a′) and (b′), we note that for both of the Si_3N_4 microcoil and carbon nanocoil there are the linear regions, i.e. an elastic spring behavior, followed by the increase in the slope. The good agreement between the theoretical and experimental results implies that the Cosserat curve model can be well used to explain the loading experiments for both the micro- and nanohelices.

Moreover, the Cosserat curve model can reveal accurately the endurance of the superelasticity behavior through F_{break}, which is the force at which failure occurred for a helix, i.e. a measure of the ability of a helix to resist the stretching force. According to the definition of the Young's modulus and Hooke's law, we have $h = h_S = EA/l_0$ at the breaking point, with h_S the spring constant of the coil wire and A the cross-sectional area of the coil wire after loading (A =

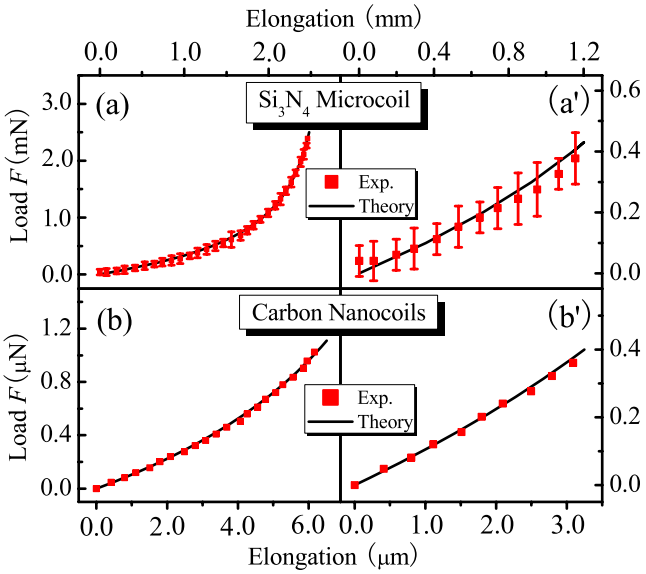

Figure 2. Theoretical calculation (solid curves) and experimental data (squares) of the load versus elongation in the low-strain region for (a) Si_3N_4 microcoil and (b) carbon nanocoil, together with the response in the linear elastic domain of the helix for (a′) Si_3N_4 microcoil and (b′) carbon nanocoil.

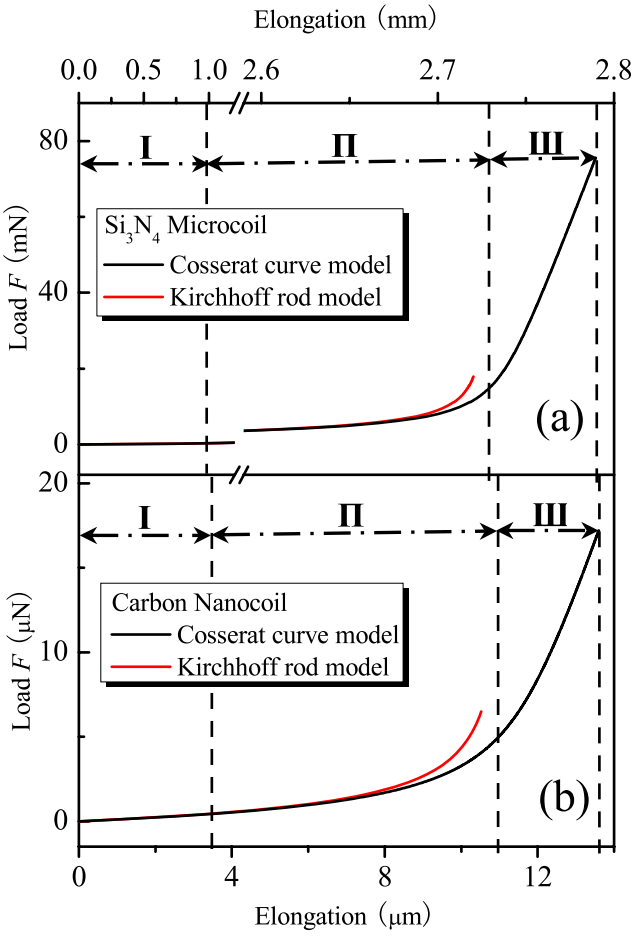

Figure 3. Load versus elongation based on the Cosserat curve model (black curves) and the Kirchhoff rod model (red curves) during the entire stretching and breaking process for (a) Si_3N_4 microcoil and (b) carbon nanocoil.

$\pi r_0^2/\lambda$). Together with equations (7), (8) and (10), we can get $F_{\text{break}} = 3.45$ GPa for the Si_3N_4 microcoil shown in figure 2(a). This result is quite reasonable compared with the deduced data from the loading experiments, which is a little larger than 2.73 GPa [7]. The ∼20% difference between our theoretical and the experimental results may be due to the assumption of a constant Young's and shear moduli during the entire loading region. In contrast, the Kirchhoff rod model fails in predicting the breaking force of the microcoil with a much smaller F_{break} of 0.82 GPa derived from equations (11) and (12) and the relation of $h = E\pi r_0^2/l_0$. For the carbon nanocoil in figure 2(b), we deduce $F_{\text{break}} = 0.52$ GPa. It is clear that the carbon nanocoil has the weaker ability to resist the stretching force than the Si_3N_4 microcoil does, consistent with the fact that the latter is harder than the former.

With the knowledge of the breaking force, we further show in figure 3 the load versus elongation of the entire stretching and breaking processes for both the Si_3N_4 microcoil and carbon nanocoil. The theoretical lineshapes obtained from equations (7) and (8) (black curves) are similar to the load–elongation curve measured by Cao *et al* [7]. We divide the load–elongation curve into three stages. Stage I is the linear elastic domain of the helix. In this region the helix is loaded by a very small force, which leads to an almost linear relationship between the force and the elongation. On strengthening the load in stage II, the elongation increases nonlinearly and the helix is pulled into a taut configuration. Stage III is a linear elastic domain of the coil wire, where the taut helix is further extended to a straight wire by a larger loading force. The force linearly follows an abrupt slope to a much higher value, which implies a huge change of the strain.

In figure 3, we have also illustrated the load–elongation curves in the Kirchhoff rod model (red curves) from equation (11). It is found that in the low-strain region, i.e. stage I and the beginning part of stage II, there is little difference between the results from the two models. However, as the elongation increases in the high-strain region, the loading force of the Kirchhoff rod model rises faster than that of the Cosserat curve model. As we know, compared with the original length of the coil wire the stretch is too small to be considered due to the small loading force in the low-strain region, the coil wire can be regarded as an inextensible and unshearable rod, i.e. the Kirchhoff rod. This assumption becomes invalid in the high-strain region, where for the same elongation the force required to extend the Kirchhoff rod of infinite resistance to shear and extension is larger than the one loading the Cosserat curve with finite E and G. Nevertheless, the Young's moduli of materials are still far smaller than infinity in the Kirchhoff rod model to determine the physical quantities, such as h_S here. That contradiction in the Kirchhoff rod model leads to the over-underestimation of the breaking force for the Si_3N_4 microcoil. Therefore, the proposed Cosserat curve model can get rid of the limitation of the traditional Kirchhoff rod model and give a complete description of the load–elongation relation for the superelasticity behavior during the entire stretching and breaking processes.

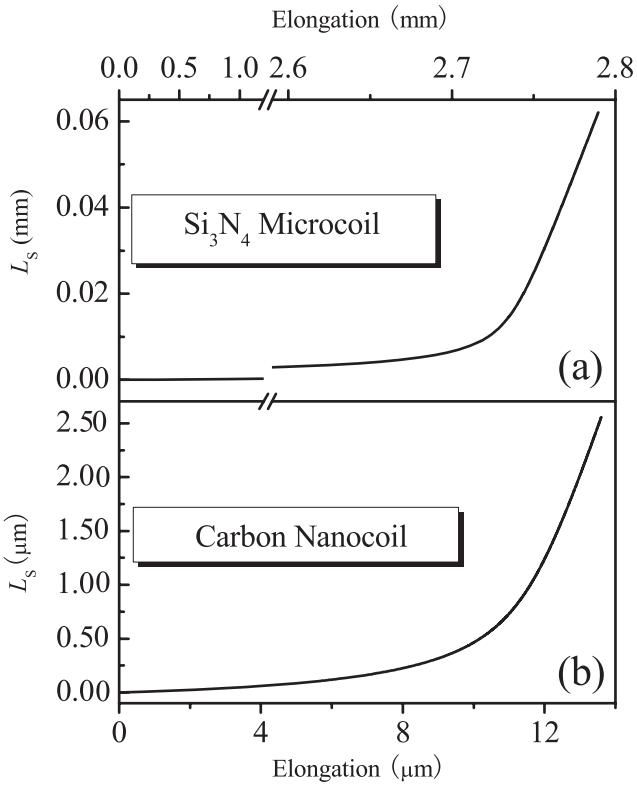

Figure 4. Elongation dependence of stretch length L_S for (a) Si_3N_4 microcoil and (b) carbon nanocoil.

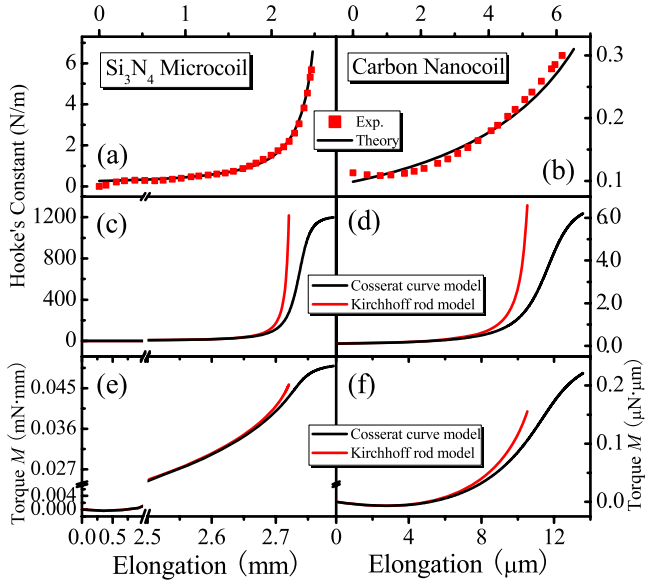

Figure 5. Theoretical calculation (solid curves) and experimental data (squares) of Hooke's constants versus elongation in the low-strain region for (a) Si_3N_4 microcoil and (b) carbon nanocoil. Hooke's constant and torque are plotted as the function of elongation based on the Cosserat curve model (black curves) and the Kirchhoff rod model (red curves) during the entire stretching and breaking process for (c), (e) Si_3N_4 microcoil, and (d), (f) carbon nanocoil, respectively.

The particular importance of the Cosserat curve model lies in the ability to deduce another important property of the superelasticity behavior, i.e. the stretch of a coil wire under the load along the helical axis. For the sake of making a detailed description of the stretch for the coil wire, we calculate the stretch length $L_S = (\lambda - 1)l_0$ based on equation (6), which reveals that L_S is determined by the loading force as well as the helical parameters. Figures 4(a) and (b) illustrate how the stretch length L_S depends on the elongation in the case of the tensile loading experiment for the Si_3N_4 microcoil and carbon nanocoil, respectively. The stretch length L_S is found to obey the accelerating rise with increasing elongation, where the linear fitted value of the growth rate $\partial L_S/\partial L$ continuously goes up from zero to almost one during the entire loading process. Judging from the definition of growth rate, it describes the relationship between the elongation ΔL and stretch length ΔL_S under the same unit change of the loading force ΔF. Including the contributions from the deformation of bending, torsion, shear and extension, ΔL is much larger than ΔL_S in the low-strain region. While up to the following extension, ΔL gets closer and closer to ΔL_S, and when the helix is pulled into a straight wire under an extremely large loading force, ΔL is equivalent to ΔL_S. The variation of the growth rate is attributed to the fact that the extension accounts for a rising portion in the deformation from a very small part to 100% in the load. Moreover, we can also learn from the stretch–load relation in figure 4 that, when the coil wires are pulled to their limit, the length of the Si_3N_4 microcoil is 1.014 times as against the unstressed state, while the carbon nanocoil extends 1.080 times. It is clear that the elongations of the coil wires are comparable to the original length, which reiterates that extension plays a key role in the high-strain region of the superelasticity behavior.

Among the various mechanical quantities of helices, the Hooke's constant enjoys obvious advantages in describing the superelasticity behavior in a direct and precise way. Figures 5(a) and (b) present Hooke's constants for the Si_3N_4 microcoil and carbon nanocoil in the low-strain region, respectively, where our theoretical Hooke's constants versus elongation reproduce well the experimental data (squares) [5, 7] by the use of equation (10) and the helical parameters in figure 2. We note that at the beginning of the load, i.e. the linear elastic domain of the helix, Hooke's constants are almost immune to the elongation, where the average values give 0.32 N m^{-1} for the Si_3N_4 microcoil and 0.12 N m^{-1} for the carbon nanocoil, in good agreement with the experimental data from the linear fit of the load–elongation curves [5, 7]. On continuing the load, the Hooke's constants are enhanced gradually with elongation. In figures 5(c) and (d), we extend the Hooke's constant to the high-strain region: Hooke's constants (black curves) increase dramatically with elongation and when the taut helices are further straightened to the breaking point they increase gently to enter in the saturation of 1198.80 N m^{-1} for the Si_3N_4 microcoil and 6.21 N m^{-1} for the carbon nanocoil, which are the spring constants of the coil wires h_S. The plateau of saturation consists with the nearly linear relation of load–elongation at the end of the loading measured by Cao *et al* [7].

To explain the Hooke's constant in the entire stretching process, we combine Hooke's constant for a helix h =

$\Delta F/\Delta L$ with the spring constant of the relevant coil wire $h_S = \Delta F \cos\zeta/\Delta L_S$, and get the expression $h = h_S \cos\zeta \frac{\Delta L_S}{\Delta L}$, with ζ the radial angle (as shown in figure 1(b)). Since the spring constant of the coil wire is assumed to be fixed, Hooke's constant is determined by the radial angle as well as the relationship of ΔL and ΔL_S revealed in figure 4. In the linear elastic domain of the helix, the deformation of the helix is rather tiny with loading force, both $\cos\zeta$ and $\Delta L_S/\Delta L$ increasing very slowly with load. Together with $\Delta L_S/\Delta L \ll 1$, the Hooke's constant therefore is small and increases slowly enough, which can be regarded as remaining the same in this region. With further extension, both $\cos\zeta$ and $\Delta L_S/\Delta L$ gradually rise to one due to conversion into a straight wire. Consequently, the elongation benefits Hooke's constant and increases it continuously to as large as the spring constant of the coil wire. It is noted that the plateau of saturation, which precisely reflects the loading characteristic near the breaking point, results from the gentle increase of $\cos\zeta$ and $\Delta L_S/\Delta L$ in that region.

Figures 5(c) and (d) also display Hooke's constants (red curves) versus elongation obtained from the Kirchhoff rod model of equation (12). It is found that the h–elongation curve strays away from that of the Cosserat curve model with a faster increase and does not exhibit the plateau of saturation in the high-strain region. If we suppose that the coil wires cannot be stretched to breaking, Hooke's constants will increase further to infinity when the elongation reaches its limits, consistent with the fact that the Kirchhoff rods have infinite resistance to shear and extension. The above analysis suggests that the hypothesis of an inextensible and unshearable rod makes the Kirchhoff rod model not suitable for describing the mechanics of the high stress acting across the cross section of the coil wires, and therefore the superelasticity characteristics of the micro-/nanohelices [5–7].

Finally, we show in figures 5(e) and (f) how the torque (equation (9)) varies with elongation for the Si_3N_4 microcoil and carbon nanocoil, respectively. It is found that at the beginning of the loads the torque decreases from zero to the minimum of negative values, and then increases continuously in the following regions (black curves). As we know, the helical torque is determined by the competition between the change of the curvature $\dot{\psi}_0 \sin\theta$ and torsion $\dot{\psi}_0 \cos\theta$, with the former decreasing from the intrinsic curvature $\psi_0' \sin\theta_0$ and the latter increasing from the intrinsic torsion $\psi_0' \cos\theta_0$ during the load. The torque–elongation curve elaborately describes the movement of the coil wire: in each loading process the helix begins from contrarotating on its axis with a negative torque followed by a clockwise revoltion. Compared with the Cosserat curve model, the Kirchhoff rod model [14] overrates the torque and misses its behavior in the linear elastic domain of the coil wire due to the assumption of infinite resistance to shear and extension (red curves). Although, as far as we know, no data are available for the experimental torque of helices, the present Cosserat curve model not only gives some important insights on the dynamics of helices from the torque point of view but also supplies a reliable reference for further experimental research.

In summary, we have shed light on the superelasticity behavior of micro-/nanohelices in the entire stretching and breaking domain by considering a Cosserat curve with four kinds of deformation of bending, torsion, extension and shear. We have derived the expressions of the mechanical quantities that allow us to predict the ability of a helix to resist stretching forces as well as the stretching of the corresponding coil wire. By quantitatively explaining all the experimental observations in the literature, we cannot only give a detailed analysis of the Hooke's constant, but also offer the experimental investigation a reliable reference for torque. In particular, it is shown that the Cosserat curve model can effectively get rid of the limitation of the traditional Kirchhoff rod model in the high-strain region through precisely describing the important superelastic mechanical properties, while the Cosserat curve model degenerated into the Kirchhoff rod model in the low-strain region by considering the rod to have infinite resistance to extension and shear. With the knowledge of the yielded mechanical properties of the superelasticity behavior in helices, our present work opens doors to the building blocks of meta-/quantum devices with a large number of potential applications in micro-/nano-engineering.

Acknowledgments

This work was supported by the Natural Science Foundation of China under contract 10734020 and the National Major Basic Research Project of 2006CB921507.

References

[1] Zhang G and Zhao Y 2004 *J. Appl. Phys.* **95** 267
[2] Gao P X, Ding Y, Mai W, Hughes W L, Lao C and Wang Z L 2005 *Science* **309** 1700
[3] Korgel B A 2005 *Science* **309** 1683
[4] Sun Y G and Rogers J A 2007 *J. Mater. Chem.* **17** 832
[5] Chen X, Zhang S, Dikin D A, Ding W, Ruoff R S, Pan L and Nakayama Y 2003 *Nano Lett.* **3** 1299
[6] Gao P X, Mai W J and Wang Z L 2006 *Nano Lett.* **6** 2536
[7] Cao C B, Du H L, Xu Y J, Zhu H S, Zhang T H and Yang R 2008 *Adv. Mater.* **20** 1738
[8] Wang Z L, Gao P X and Ding Y 2005 *US Patent Pending*
[9] Goriely A and Tabor M 1998 *Phys. Rev. Lett.* **80** 1564
[10] McMillen T and Goriely A 2002 *J. Nonlinear Sci.* **12** 241
[11] Schlick T 1995 *Curr. Opin. Struct. Biol.* **5** 245
[12] Olson W K 1996 *Curr. Opin. Struct. Biol.* **6** 242
[13] Goldstein R E and Langer S A 1995 *Phys. Rev. Lett.* **75** 1094
[14] da Fonseca A F and Galvão D S 2004 *Phys. Rev. Lett.* **92** 175502
[15] Chouaieb N, Goriely A and Maddocks J H 2006 *Proc. Natl Acad. Sci. USA* **103** 9398
[16] Whitman A B and DeSilva C N 1974 *J. Elast.* **4** 265
[17] Cosserat E and Cosserat F 1909 *Theorie des Corps Deformables* (Paris: Hermann)
[18] Love A E H 1944 *A Treatise on the Mathematical Theory of Elasticity* (New York: Dover)
[19] Zhou Z, Lai P Y and Jos B 2005 *Phys. Rev.* E **71** 052801
[20] Hutchinson J R 2001 *J. Appl. Mech.* **68** 87
[21] Fate W A 1975 *J. Appl. Phys.* **46** 2375